Resonant Raman scattering in diamond

J. M. Calleja,* J. Kuhl, and M. Cardona
Max-Planck-Institut für Festkörperforschung, 7000 Stuttgart 80, Federal Republic of Germany
(Received 20 June 1977)

The first- and second-order Raman scattering have been investigated in diamond below but near the fundamental gap using a frequency doubler for the high-photon-energy region. No resonance was found for the first-order Raman scattering up to 4.8 eV, while the second-order spectrum was clearly resonance enhanced as the gap was approached. These facts are explained as the result of the interference of the contributions to the first-order Raman cross section from the E'_0 and E_2 gaps resulting in a cancellation for the dispersion of the first-order Raman scattering. Explicit expressions for the E_0' and E_2 contributions to the first-order absolute Raman tensor (which turns out to be negative) are given. The electron–one-phonon deformation potentials at the Γ and X points which appear in these expressions are evaluated in analytic form by using pseudopotential theory. The absolute scattering cross sections so obtained are compared with experimental values reported in the literature. An electron–two-phonon deformation potential for the E_0' gap is determined.

I. INTRODUCTION

Diamond, perhaps the best prototype of a covalent crystal, is an ideal material for Raman scattering experiments. This is mainly due to the hardness of the crystal (i.e., the high frequency of the phonons), and to the fact that it is transparent in the visible and the near-uv region. Consequently a vast amount of information on diamond has been obtained since the first Raman experiments,[1,2] the most recent work giving an exhaustive assignment of the features of the first- and second-order Raman spectra[3] and the Brillouin scattering.[4] Speculations about the possible existence of a two-phonon bound state at the cutoff of the second-order Raman spectrum[3,5-7] and the experimental determination of the absolute first-order Raman cross section[4,8] are perhaps the highlights of the most recent work. While the magnitude of this cross section is in reasonable agreement with theoretical predictions[6,9,10] and indirect experimental estimates,[11] the sign of the first-order Raman tensor has not yet been established (see Sec. IV A and Table I). Swanson and Maradudin[10] made a pseudopotential calculation of the first-order Raman tensor for Si, Ge, and diamond, including terms up to sixth order in the exciting frequency and found that these frequency-dependent terms were nearly negligible for diamond.

Resonant Raman scattering has been studied in many tetrahedral compounds (e.g.,[12] Ge and[13] Si) but not yet in diamond because its fundamental gap (6 eV) cannot be approached with standard lasers. We have succeeded in measuring the dependence on photon energy of the first- and second-order Raman scattering below but near the gap using an Ar^+ and a rhodamine 6G dye laser in conjunction with a frequency doubler. The efficiency of the first-order Raman scattering was found to remain constant in the frequency region under investigation (2–4.8 eV) in agreement with the calculations of Swanson and Maradudin.[10] The second-order scattering, however, resonates clearly as the gap is approached. These results are explained as due to an interference of two scattering mechanisms. One of them involves the lowest direct gap (E_0') and the other corresponds to a higher gap, vaguely referred to as E_2 in the literature.[6] A simple pseudopotential calculation of the electron–one-phonon deformation potentials of the states forming the E_0' and E_2 gaps has been made. The E_0' gap occurs at the Γ point. The E_2 gap has been assumed to occur at the X point of the Brillouin zone. Expressions for these deformation potentials are given in analytic form. The E_0' first-order deformation potentials combined with the absolute measurements of Grimsditch and Ramdas[4] enable us to explain the lack of resonance in the first-order Raman scattering. However, the deformation potentials calculated at the X point are too small to explain the magnitude of the E_2 contribution to the Raman cross section and to the elasto-optical constants extracted from the experiment, a

TABLE I. Absolute first-order Raman tensors $P^{(1)}$ of diamond (Å^2) as obtained experimentally (a,d,e,g) and theoretically (b,c,f).

3.4–4.4 [a]	+3.5 [b]	−1.82 [c]	4.6 [d]
4.4 [e]	−3.8 [f]	−2.5 [g]	

[a] Reference 11.
[b] Reference 6.
[c] Reference 10.
[d] Reference 8.
[e] Reference 4.
[f] Reference 9. Note that according to Ref. 4 this calculation contains errors.
[g] This work.

TABLE II. Experimental configurations used and corresponding Raman allowed modes. H and V refer to polarizations parallel (horizontal) and perpendicular (vertical) to the scattering plane, respectively.

Configuration	Raman
I_V^V	$A_{1g}+T_{2g}+E_g$
I_H^V	$\frac{2}{3}T_{2g}+E_g$
I_H^H	$\frac{1}{3}T_{2g}+2E_g$
I_V^H	$\frac{1}{3}T_{2g}+2E_g$

fact which reflects the extended nature of the electronic transitions involved in the E_2 gap.[14]

In Sec. II we describe the experimental details and particularly the technique used for frequency doubling. The experimental results, together with the corresponding theoretical fits, are displayed in Sec. III. Section IV contains the discussion of the experimental results in terms of the proposed model; expressions for the E_0' and E_2 contribution to the first-order Raman scattering are given in Sec. IV A. The explicit expressions for the electron–one-phonon deformation potentials involved in Sec. IV, as well as their numerical values for diamond, are given in the Appendix.

II. EXPERIMENTAL DETAILS

All the data presented here were obtained on a $3\times3\times2$-mm^3 diamond parallelepiped of type IIa. Right-angle scattering geometry was used. The directions of the incident and scattered light were $(2,-3,1)$, and $(1,1,1)$, respectively, because the orientation of the available sample did not allow any simpler configurations. We shall denote the four configurations studied as I_V^V, I_H^V, I_V^H, I_H^H, where the superscript stands for the polarization direction of the incident light and the subscript for that of the scattered light, and V and H mean perpendicular and parallel to the horizontal scattering plane, respectively. These configurations allowed us to observe the Raman modes listed in Table II. The Raman-active optical phonon at 1332 cm^{-1} has T_{2g} symmetry. In second order, T_{2g}, E_g, and A_{1g} modes exist in principle, but the E_g modes have been found to be nearly negligible.[3] The T_{2g} component amounts to only $\frac{1}{3}$ of A_g.[3]

In the spectral range from 6471 to 3250 Å (1.91 to 3.82 eV) the lines of Spectra Physics Models 171 and 185 lasers (Kr^+ and He-Cd, respectively) were used. Owing to the lack of cw-laser emission lines at wavelengths shorter than the 3250-Å line of the He-Cd laser, we had to develop frequency-doubling accessories for the 5145-Å line of an Ar^+ laser and the yellow emission of a cw rhodamine 6G dye laser. These devices allowed extension of the measurement range up to 4.2-eV (2956-Å) and 4.82-eV (2574-Å) excitation photon energies, respectively. Efficient cw conversion of visible laser radiation to the uv region was achieved by intracavity second-harmonic generation (SHG). The resonator configuration employed for frequency doubling of the Ar^+ laser line has been described earlier by Huber[15] (see Fig. 1). The output mirror of the laser was removed and the resonator was extended to a folded-three-mirror cavity. The ammonium dihydrogen phosphate (ADP) crystal (50 mm long) was mounted at the position of the beam waist between the two spherical mirrors. The surfaces were cut for Brewster's angle of incidence at the fundamental frequency and highly polished to minimize laser cavity losses introduced by insertion of the frequency doubler. These losses can severely limit the conversion efficiency. 90°-phase-matched SHG of the 5145-Å line, which yields optimum conversion efficiency in ADP, requires a crystal temperature of −11 °C. Cooling of the crystal and stabilization of its temperature within ±0.02 °C was obtained by a Peltier cooler controlled by a platinum resistance thermometer. Efficient extraction of the second harmonic from the laser cavity was made possible by the spherical mirror M which was coated with special dielectric layers highly reflecting at 5145 Å (R >99.5%) and transmitting more than 80% at 2572 Å. This device yields typical cw output between 20 and 40 mW. The output power was determined by means of a calibrated Si photodiode. It should be pointed out that this uv output was already obtainable at relatively low ion laser current levels (≃25–30 Å). Further increase of the tube current or fundamental power within the cavity yields no noticeable improvement. This saturation of the uv output may be explained by thermally induced variation of the optical properties of the ADP crystal. Even small temperature gradients within the nonlinear material prevent exact phase matching and therefore reduce the second-harmonic power. Moreover, thermally induced losses in the crystal decrease the Q factor of the resonator.

Intracavity SHG of the rhodamine 6G dye laser radiation was performed in a 90°-phase-matched ammomium dihydrogen arsenate (ADA) crystal (30 mm long). The flat out put mirror of the usual folded-three-mirror cavity was replaced by an antireflectance (AR) coated lens (f = 50 mm) and a spherical mirror of 100 mm radius of curvature. The nonlinear crystal mounted in a temperature-stabilized oven was located at the beam waist position between these two elements. The spherical mirror, which was transparent in the uv and highly reflecting in the visible range, served as the out-

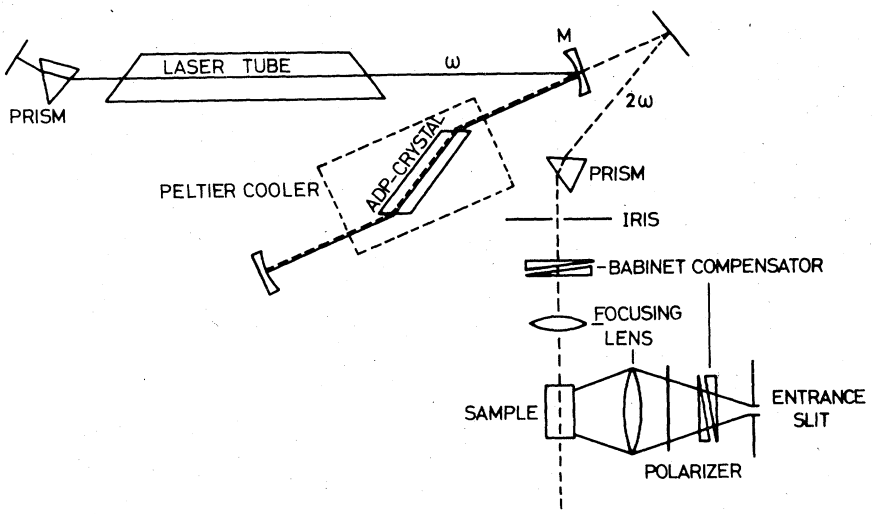

FIG. 1. Experimental setup for light scattering measurements with the frequency doubler. The solid line indicates the pumping beam, while the dashed line stands for the doubled beam.

put coupler. The bandwidth of the dye laser was narrowed by a three-element birefringent filter and an additional Fabry Perot etalon (0.1-mm thick quartz plate, coated with dielectric mirrors $R \simeq 65\%$) to about 10 GHz. For $\lambda = 2956$ Å, typical uv outputs of 5–10 mW were obtained at a crystal temperature of 45 °C. The conversion rate was severely limited by thermal instabilities of the nonlinear material. However, as Fröhlich *et al.* have demonstrated,[15] an improvement of the uv output at least by a factor of 5 is obtainable with less absorbant nonlinear crystals and a resonator configuration which carefully minimizes the total cavity losses.

We used Babinet compensators before and after the sample to obtain all the configurations of Eq. (1) keeping the polarization of the light entering into the monochromator parallel to the ruling of the gratings. In this way, the sensitivity of our detection system (a $\frac{3}{4}$-m SPEX double monochromator with 1800 g/mm holographic gratings and a RCA C31034 A photomultiplier) was maximum for the near-uv (3000 Å) region. Because of the wide range of the recorded Raman spectra (up to 3000-cm^{-1} shift) and of the fact that the sensitivity of our equipment (photomultiplier, grating efficiency) decreased rapidly with increasing photon energy in the region where the frequency doubler was used, special care was required for the determination of scattering efficiencies. It was necessary to know as accurately as possible the throughput function of the system as a function of frequency, even for measurements made relative to a CaF_2 crystal (the Raman shifts of CaF_2 and diamond are vastly different). With this in mind, a calibration of the whole monochromator and detection system was made using a deuterium lamp previously calibrated by the Max Planck Institute for Astronomy at Deutsches Elektronen-Synchrotron (DESY), Hamburg, using synchrotron radiation. The sensitivity of our system for Stokes shifts between 0 and 3000 cm^{-1} changed by factors of 7.5 and 2.7 for 2572- and 2956-Å excitation wavelength, respectively. The first-order Raman peak (1332-cm^{-1} Stokes shift) was first measured relative to the CaF_2 peak (320-cm^{-1} shift) in the whole spectral range for all the configurations of Eq. (1) and then (see Sec. III) the second-order spectra were measured relative to the first-order peak. In all the cases the data were corrected for the throughput of the monochromator detection system, the absorption of the sample, the ω^4 factor, and the laser power. Typical slit widths were 200 μ. The effects of the variation of the resolution with wavelength were corrected for. All measurements were carried out at room temperature.

III. RESULTS

The spectra obtained in this work are basically the same as those of Fig. 3(a) in Ref. 3, the only differences being those imposed by the selection rules of Table II. In Fig. 2 we present three second-order Raman spectra recorded for different excitation wavelengths in the I_V^V configuration. Although a clear increase in the scattered intensity with increasing excitation energy appears, no significant changes in the shape of the spectrum are observed except for the small peak at 2290 cm^{-1}, which could be ascribed to a $L(X_1) + TO(X_4)$ combination.[3,16] This peak could be understood as a resonance effect[17] since the lowest indirect gap in diamond occurs at the X point.[18] No resonance enhancement of the $2TO(\Gamma)$ peak similar to that seen near the E_1 gap of[12] Ge and[13] Si was observed. It would be very interesting to extend our photon energies to $\simeq 6$ eV in order to see whether such reso-

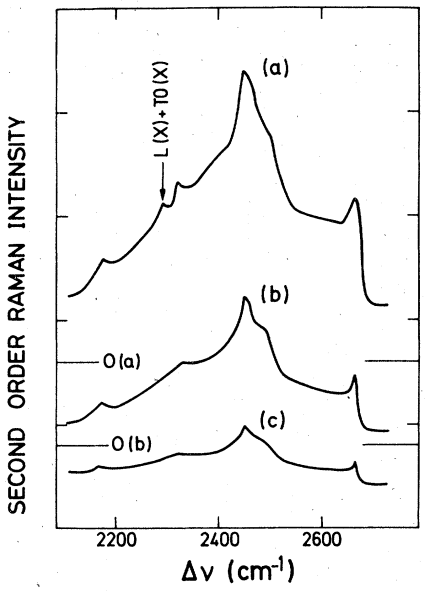

FIG. 2. Second-order Raman spectra for several exciting frequencies in I_V^V configuration. The ordinate is in arbitrary units, which, however, are the same for all the spectra. The zero of curves (a) and (b) has been shifted for the sake of clarity. The exciting frequencies are (a) 2572 Å, (b) 3250 Å, and (c) 5682 Å.

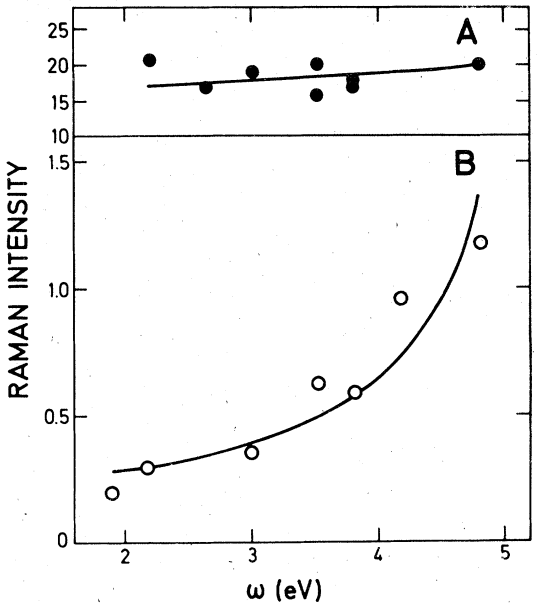

FIG. 3. (a) First-order Raman-integrated intensity, normalized to CaF_2, versus exciting frequency. The solid line is the least-squares fit to the experimental points with Eq. (1). (b) Second-order Raman-integrated intensity, normalized to the first-order one, versus exciting frequency. The solid line is the least-squares fit to the points with Eq. (3). Both (a) and (b) have been taken in I_V^V configuration.

nance also occurs near the E_0' gap of diamond or whether it is characteristic of E_1 gaps.

We did not find any resonance enhancement in the first-order Raman cross section in the frequency range studied, as can be seen in Fig. 3(a). In this figure, we have plotted laser frequency (full circles) versus the first-order Raman-integrated intensity divided by that of the CaF_2. The gap of CaF_2 is approximately 11 eV and therefore this material is not expected to have any resonance in the region of our measurements. The solid line is the least-squares fit to the experimental points with the results of the calculation of Swanson and Maradudin[10] for the first-order Raman efficiency:

$$I^{(1)} = C(P_0 + P_1\omega^2)^2, \tag{1}$$

where P_0, the independent component of the Raman tensor at $\omega = 0$, equals 1.78 Å^2 and $P_1 = -0.008$ Å eV^{-2}, ω is the laser frequency in eV, and C an adjustable parameter determined by the ratio of the absolute cross section of diamond to that of CaF_2. The least-squares-fitting procedure yields $C = 5.3$. In Fig. 3(b) the integrated intensity of the second-order structure shown in Fig. 2, relative to the first-order one, both in I_V^V configuration, is plotted versus exciting frequency. The solid line is the least-squares fit to the experimental data (open circles) with the equation appropriate to the Γ_1 component of the Raman efficiency,[19]

$$I^{(2)} = A[g(x) + 3f(x) + B]^2, \tag{2}$$

where

$$g(x) = x^{-2}[2 - (1-x)^{-1/2} - (1+x)^{-1/2}],$$

$$f(x) = x^{-2}[2 - (1-x)^{1/2} - (1+x)^{1/2}],$$

and $x = \omega/\omega_0$, ω_0 being the lowest direct gap ($E_0' \simeq 6$ eV[14]). The adjustable parameters A and B are 1.5 and −0.4, respectively, for the least-squares fit.

IV. DISCUSSION

A. First-order Raman scattering

As shown in Fig. 3(a), the lack of resonance observed for the first-order Raman scattering agrees well with the computer calculations of Swanson and Maradudin[10] based on the pseudopotential band structure of diamond. This behavior is contrary to the observations for the lowest direct gap of other zinc-blende–type semiconductors.[19] This gap, however, is usually E_0 ($\Gamma_{25'} \rightarrow \Gamma_{2'}$) while that of diamond is E_0' ($\Gamma_{25'} \rightarrow \Gamma_{15}$). One may therefore be inclined to compare diamond with silicon which has an E_0' lowest direct gap with a strong reso-

nance of the first-order Raman scattering.[13] For silicon, however, the E_0' gap is nearly degenerate with E_1,[19] a fact which does not obtain for diamond.[18] Two possible explanations of the lack of first-order resonance found in diamond can be given: either the contribution of the E_0' gap is fortuitously small (small deformation potentials) or its dispersion is canceled, to the order in ω^2 relevant to our experimental region, by the contribution of higher gaps (which are usually loosely labeled[19] E_2 and located[18] at around 12 eV for diamond). In the latter case, an antiresonance would be expected as the laser frequency is increased beyond our experimental limit (4.8 eV) towards E_0' $\simeq$6 eV. Unfortunately, in the computer calculations of Ref. 10 no attempt was made to separate the E_0' contributions from the background and thus to solve theoretically the present dilemma. We shall present here a simple microscopic model to calculate the E_0' contribution and to estimate that of E_2. According to this model the E_0' contribution is not negligible and an antiresonance in the first-order Raman cross section would be expected as ω_0 is increased beyond 4.8 eV. The lack of antiresonance shown in Fig. 3 is then interpreted as due to a cancelation of the ω^2 terms in the expansion of the E_0' and E_2 contributions to the Raman tensor.

We assume that the E_0' gap corresponds to transitions between a threefold degenerate valence band ($\Gamma_{25'}$) and a threefold degenerate conduction band, all parabolic. The first-order Raman scattering is then produced by the electron-phonon interaction of the T_{2g} ($\equiv\Gamma_{25'}$) phonons with the $\Gamma_{25'}$ and Γ_{15} bands. This electron-phonon interaction is characterized by the deformation potential d_0 and d_0^{15}, defined in Ref. 19. Explicit expressions for d_0 and d_0^{15} as a function of the pseudopotential form factors are given in the Appendix. The values calculated for diamond are given in Table IV. The contribution to the Raman tensor $P^{(1)}(E_0')$ is obtained as the effect of a sublattice displacement (T_{2g} phonon) $\frac{1}{4}a_0(\delta,0,0)$ on the electric susceptibility tensor χ (a_0 is the lattice constant). A simple calculation[19] yields

$$P^{(1)}(E_0') = \lim_{\delta\to 0}(a_0^2/\delta)\,\chi_{xy}(\omega) = \frac{\sqrt{3}a_0^2}{16}(d_0^{15}-d_0)\,\frac{d\chi}{d\omega_0}\,, \tag{3}$$

where ω_0 stands for the frequency of the E_0' gap. It is customary to use for χ and $d\chi/d\omega_0$ the analytic expressions for parabolic bands extending to infinity:

$$\chi = (c_0''/4\pi)f(x)\,, \tag{4a}$$

$$\frac{d\chi}{d\omega_0} = \frac{c_0''}{8\pi\omega_0}g(x)\,, \tag{4b}$$

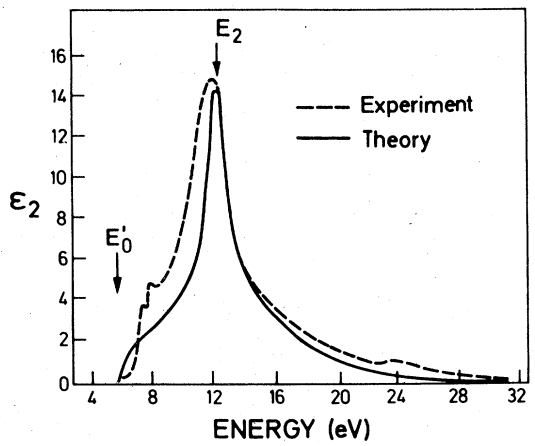

FIG. 4. Imaginary part of the dielectric constant for diamond versus frequency. The E_0' and E_2 gaps are indicated by arrows. (From Ref. 14).

with $f(x)$ and $g(x)$ defined in Eq. (2). By fitting the region between 6 and 8 eV of Fig. 4 with the imaginary part of Eq. (4a) we obtain $c_0''=6$.

For the E_2 transitions we use essentially the Penn model[20] related, in the framework of pseudopotential theory, to the X_4-X_1 gap.[21] Within this model the E_2 contribution $P^{(1)}(E_2)$ arises from the phonon-induced splitting of the X_1 conduction-band degeneracy, the corresponding splitting of the X_4 valence band being zero (see the Appendix). In terms of the phonon deformation potential $\mathcal{E}_{2,0}^{*}$ for X_1 (see Appendix and Ref. 22) the Raman-tensor contribution $P^{(1)}(E_2)$ can be written as

$$P^{(1)}(E_2) = -\frac{a_0^2}{8}\mathcal{E}_{2,0}^{*}\,\frac{d\chi}{d\omega_2}\,. \tag{5}$$

The E_2 contribution to χ can be approximated (see Fig. 4) by a harmonic oscillator of frequency $\omega_2\simeq$12 eV:

$$4\pi\chi(E_2) = D/(\omega_2^2-\omega^2)\,. \tag{6a}$$

From the low-frequency value of the dielectric constant[19,23] $\epsilon(0)=5.6$ and Eqs. (4a) and (6a) we obtain for D the value 454 eV^2. Thus we can write, to terms of second order in ω/ω_2:

$$\frac{d\chi}{d\omega_2} = -\frac{227}{\pi\omega_2^3}\left(1+2\,\frac{\omega^2}{\omega_2^2}\right). \tag{6b}$$

Using the values of the deformation potentials given in Table IV and Eqs. (4b) and (6b), we can evaluate Eqs. (3) and (5). [It is actually sufficient to use the Taylor expansion of $g(x)$ up to quadratic terms in x except very near the gap.] We obtain (in Å^2)

$$P^{(1)}(E_0') \simeq 5.5 + 0.11\,\omega^2\,, \tag{7a}$$

$$P^{(1)}(E_2) \simeq -2.3 - 0.032\,\omega^2. \tag{7b}$$

Equation (7b) has been obtained under the assumption that the structure of the electron-phonon interaction of the E_2 transitions corresponds exclusively to transitions at the X point. As already mentioned, the E_2 transitions occur over a wide region of the Brillouin zone where other deformation potentials are bound to be operative. Hence Eq. (7a) is expected to be considerably more accurate than Eq. (7b). Nevertheless, the coefficient of the ω^2 term in Eq. (7b) already suggests the possibility of a dispersion cancelation between Eqs. (7a) and (7b). In order that this cancelation takes place we multiply Eq. (7b) by an *ad hoc* factor of 3.4. While this factor is large, we remind the reader that the phonon deformation potential at X_4 is accidentally zero, and that $\mathcal{S}_{20}$ is relatively small (compare it with d_0 in Table IV). Upon multiplication of $P^{(1)}(E_2)$ by 3.4 in Eq. (7b) we find:

$$P^{(1)} = P^{(1)}(E_0') + P^{(1)}(E_2) = -2.4\ \text{Å}^2. \tag{8}$$

The magnitude of $P^{(1)}$ given in Eq. (8) agrees reasonably with experimental determinations (see Table I). The sign of $P^{(1)}$ has not been previously determined experimentally and, if the theoretical manipulations given here are trusted, the result of Eq. (8) can be construed as an experimental determination of the sign of $P^{(1)}$. The negative sign agrees with the calculations of Refs. 9 and 10 but not with those of Ref. 6. We have therefore reexamined the origin of the "+" sign in $P^{(1)}$ in the work of Ref. 6 and found it to be based on the strength of the extremely weak E_g (Γ_{12}) component of the second-order Raman tensor (10^3 times smaller than the T_{2g} and the A_{1g} components).

Under these conditions, the experimental determination of the E_g component is not reliable (what one observes is likely to be due to misalignments). If one assumes in the analysis of Ref. 6 that the E_g component vanishes, one obtains a negative value of $P^{(1)}$, in agreement with all other sign determinations. We thus conclude that the sign of the Raman tensor $P^{(1)}(\omega = 0)$ of diamond, unlike that of germanium[10] and silicon,[10,24] is negative.

B. Second-order Raman scattering

The second-order Raman cross section is clearly resonance enhanced when the exciting frequency approaches the E_0' gap [see Fig. 3(b)]. This enhancement is well described by Eq. (2), in which $g(x) + 3f(x)$ represents the derivative of the electric susceptibility with respect to a cubic perturbation of A_{1g} symmetry (note that $g + 3f = 0$ for $x = 0$) corresponding to the symmetry of the second-order Raman effect, which is mostly Γ_1.[3] The fit parameter $B \simeq -0.4$ stands for the nondispersive contribution of gaps higher than E_0'. Due to the relatively small value of B we can conclude that most of the resonant behavior of the second-order Raman scattering must be ascribed to the E_0' gap. Higher gaps have only a small and nondispersive contribution, in contrast to the situation for first-order scattering. The only resonance effect which could be ascribed to the E_2 gap (X point) is the appearance of the small peak at the $L(X) + \mathrm{TO}(X)$ position with 2572-Å exciting wavelength (see Fig. 2).

The functional dependence of Eq. (2) enables us to conclude that the two-phonon scattering takes place mainly via a renormalized electron–two-phonon interaction. An enhancement of two-Γ-phonon structure due to resonant iterated electron–one-phonon processes, of the type observed in[12] Ge and[13] Si, is not seen. This emphasizes the fact that the peak observed at the frequency of two $O(\Gamma)$ phonons in Fig. 2 (high-frequency cutoff) is not due to double resonance. Once the possibility of a two-phonon bound state has been ruled out,[6,7] the effects of density of states[7] and energy-dependent matrix elements[6] remain as the only possible explanation.

The spectrum of Fig. 2 is due almost exclusively to scattering by the LO and TO branches which are extremely flat.[3,16] Since the A_{1g} component is dominant we assume that, as in the case of germanium[12] and silicon,[13] the two-phonon spectrum of Fig. 2 consists mainly of overtones. Under these conditions it is possible to obtain from the data of Fig. 3(b) and the electron–one-phonon deformation potentials d_0 and d_0^{15} of Table IV the electron–two-phonon average deformation potential $D_1(E_0')$ for the E_0' gap which determines the integrated scattering efficiency for two-optical-phonon scattering[25] through the Raman-tensor component a (in Loudon's notation[26]):

$$a^{(2)}(E_0') = \frac{c_0'' D_1(E_0')}{12 a_0^2 \omega_0' \pi} \langle n_1 + 1 | u_1 | n_1 \rangle \times (g + 3f)(2\eta N)^{1/2}, \tag{9}$$

where η is the degeneracy factor, equal to 3 if LO and TO phonons are involved,[16] u_1 is the displacement of the appropriate phonon, n_1 is the corresponding occupation number (at room temperature, $n_1 \simeq 0$), and N is the number of unit cells participating in the scattering. The efficiency for T_{2g} first-order scattering is determined by the Loudon-tensor component d[19]:

$$d(E_0') = \frac{8}{a_0^3} P^{(1)}(E_0') \langle n_0 + 1 | u_0 | n_0 \rangle = \frac{\sqrt{3}\, c_0''}{16 a_0 \omega_0' \pi} (d_0^{15} - d_0)\, g(x) \langle n_0 + 1 | u_0 | n_0 \rangle . \tag{10}$$

According to Table II, in the I_V^V configuration of Fig. 3 the ratio of second-order to first-order efficiencies is given by $(a/d)^2$. Using Eqs. (7a) and (7b) we thus find from the fit of Fig. 3

$$|a(E_0')/d(E_0')| = 0.53(-g-3f), \quad \omega \to 0. \tag{11}$$

Combining Eq. (11) with Eqs. (9) and (10), and using the expression

$$\langle n+1|u|n\rangle = (1/4MN\Omega)^{1/2}, \tag{12}$$

where M is the atomic mass, N is the number of unit cells for unit volume, and Ω is the phonon frequency, we find

$$D_1(E_0')/(d_0 - d_0^{15}) = 36, \tag{13}$$

and using the deformation potentials d_0 and d_0^{15} of Table IV

$$D_1(E_0') = 4800 \text{ eV}. \tag{14}$$

The ratio of second- to first-order deformation potentials given in Eq. (12) is similar to that found in many semiconductors.[12,13,25] The absolute value of (E_0') given in Eq. (14), however, is much larger than usual (typically ~2000 eV) for tetrahedral semiconductors). This reflects the fact that the first-order deformation potentials of diamond are also larger than usual (see Table IV and Refs. 2, 13, and 25). As can be seen in the Appendix, this is a result of the large pseudopotential form factors of diamond.

V. CONCLUSIONS

The dependence on laser frequency of the efficiency of diamond for scattering by one and two phonons has been studied in the region from 2 to 4.8 eV. In agreement with earlier pseudopotential calculations of the first-order Raman tensor, the corresponding scattering efficiency is found to be nonresonant in the experimental region. This fact is attributed to a cancelation of the resonant contributions of the E_0' and E_2 gaps. An evaluation of these contributions, and some manipulations to bring the E_2 contribution into agreement with the experimental observations, lead to a *negative* value for the long-wavelength Raman tensor. The observed second-order resonance is interpreted in terms of an electron–two-phonon deformation potential $D_1(E_0')$ = 4800 eV. An indication of an "indirect" resonance at the $\Gamma \to X$ indirect gap, for the $L(X) + \mathrm{TO}(X)$ phonon combination has been observed.

ACKNOWLEDGMENTS

We would like to thank M. H. Grimsditch for stimulating discussions, W. Holzapfel for supplying the diamond sample, and E. Pitz for the calibration of the deuterium lamp.

APPENDIX

It has been shown,[19,22] that in materials with zinc-blende structure the Γ_{15} conduction pseudo wave function can be expressed as appropriate symmetrized linear combinations of $\langle 111\rangle$-plane waves with coefficients β and γ, respectively, which are obtained as the eigenvectors of a 2×2 matrix [see Eq. (43) of Ref. 19]. With the pseudopotential form factors v_i of Table III we find $\beta = 0.84$ and $\gamma = 0.54$. The splitting of the $\Gamma_{25'}$ and Γ_{15} bands for a $\Gamma_{25'}$ phonon is represented by the deformation potentials d_0 and d_0^{15}, respectively. Details about the application of the pseudopotential method to calculating deformation potentials, including tables of symmetrized wave functions and deformation potentials, are given in Ref. 22 (note that the corresponding deformation potentials of this reference are defined to be a factor of 3 larger). We find[22]:

$$\begin{aligned} d_0 &= -(4\pi/\sqrt{3})[\beta^2(v_4 - v_{12}) + \sqrt{2}\beta\gamma(v_3 - v_{11})] \\ d_0^{15} &= (4\pi/\sqrt{3})(v_4 - v_{12}), \end{aligned} \tag{A1}$$

where $\Omega = (2\pi/a_0)^2$ with a_0, the lattice constant, expressed in bohrs, ζ is the internal stress parameter ($\simeq 0.22$ for diamond[28]), and v_i' are the derivatives of v_i with respect to $\ln G$ ($\vec{G}$ is a reciprocal-lattice vector, energies in Ry). At the $X(100)$ point the X_4 valence band can be written in the simplest possible model as a symmetrized combination of $\langle 100\rangle$ waves

$$X_4 \times \begin{cases} (1/\sqrt{2})([011] + [0\bar{1}\bar{1}]) \\ (1/\sqrt{2})([0\bar{1}1] - [01\bar{1}]). \end{cases} \tag{A2}$$

The two X_1 conduction bands can be written as linear combinations of the symmetrized $\langle 011\rangle$ and $\langle 100\rangle$ waves with coefficients β_x and γ_x which are obtained as the eigenvectors of Eq. (34) of Ref. 19. For diamond, we find with the v_i and v_i' of Table III (Ref. 27) $\beta_x = 0.81$ and $\gamma_x = -0.58$. The splitting of the X_1 states due to a $\Gamma_{25'}$ phonon is given by the $\mathcal{S}_{20}^*$ deformation potential, whose expression in terms of the pseudo wave functions given above is

TABLE III. Pseudopotential form factors $v(G)$ and their logarithmic derivatives $v'(G)$ for diamond (Ry). The values have been obtained by drawing a smooth curve through the experimental points given in Ref. 27.

	$v(G)$	$v'(G)$
v_3	−0.81	2.93
v_4	−0.40	2.74
v_8	0.34	0.00
v_{11}	0.13	−2.03
v_{12}	0.04	...

TABLE IV. Deformation potentials (eV) for an optical phonon [$d_0(\Gamma_{25'})$, $d_0^{15}(\Gamma_{15})$, and $\mathcal{E}_{20}^{*}(X_1)$] calculated with the v_i and v_i' of Table III and Eqs. (A1) and (A3).

Γ	d_0	d_0^{15}
	90.1	−43.4
X	$\mathcal{E}_{20}^{*}$	
	−34.5	

$$\mathcal{E}_{20}^{*} = -2\pi(\sqrt{2}\beta_x\gamma_x v_3 + \gamma_x^2 v_4)\,. \tag{A3}$$

The corresponding splitting of the X_4 valence bands of Eq. (A2) is proportional to the v_s' pseudopotential coefficient, which is zero for diamond (see Table III). Thus the X_4 bands remain degenerate (the corresponding deformation potential is zero). The deformation potentials obtained with Eqs. (A1) and (A3) using the v_i and v_i' of Table III are listed in Table IV. The explicit expressions for the deformation potentials given in this Appendix can also be used for Ge and Si and, to a good approximation, for III–V semiconductors. Equation (A3) with $\beta_x = 0.89$ and $\gamma_x = -0.46$, and the pseudopotential form factors of Ref. 19, yields for Si $\mathcal{E}_{20}^{*} = -8.2$ eV. This number agrees with experimental data.[29] The value $\mathcal{E}_{20}^{*} = 2$ eV given in Ref. 30, calculated with the same technique as used here, is the result of a computational error.

*Supported in part by the Alexander von Humboldt Foundation; present address: Universidad Autonoma de Madrid, Facultad de Ciencias, Madrid, Spain.

[1]C. V. Raman, Proc. Indian Acad. Sci. A 44, 99 (1956).
[2]D. Krishnamurti, Proc. Indian Acad. Sci. A 40, 211 (1954), and Refs. therein.
[3]S. A. Solin and A. K. Ramdas, Phys. Rev. B 1, 1687 (1970).
[4]M. H. Grimsditch and A. K. Ramdas, Phys. Rev. B 11, 3139 (1975).
[5]J. Ruvalds and A. Zawadowsky, Phys. Rev. B 2, 1172 (1970).
[6]S. Go, H. Bilz, and M. Cardona, Phys. Rev. Lett. 34, 580 (1975).
[7]R. Tubino and J. L. Birman, in *Light Scattering in Solids*, edited by Balkanski, Leite, and Porto (Flammarion, Paris, 1976), p. 419.
[8]A. K. McQuillan, W. R. L. Clements, and B. P. Stoicheff, Phys. Rev. A 1, 628 (1970).
[9]A. A. Maradudin and E. Burstein, Phys. Rev. 164, 1081 (1967).
[10]L. R. Swanson and A. A. Maradudin, Solid State Commun. 8, 859 (1970).
[11]E. Anastassakis and E. Burstein, Phys. Rev. B 2, 1952 (1970).
[12]M. A. Renucci, J. B. Renucci, R. Zeyher, and M. Cardona, Phys. Rev. B 10, 4309 (1974).
[13]J. B. Renucci, R. N. Tyte, and M. Cardona, Phys. Rev. B 11, 3885 (1975).
[14]A. R. Lubinsky, D. E. Ellis, and G. S. Painter, Phys. Rev. B 6, 3950 (1972).
[15]P. Huber, Opt. Commun. 15, 196 (1975); D. Fröhlich, L. Stein, and H. Welling, Appl. Phys. 11, 97 (1976).
[16]J. L. Warren, J. L. Yarnell, G. Dolling, and R. A. Cowley, Phys. Rev. 158, 805 (1966).
[17]J. S. Kline, M. Masui, J. J. Song, and R. K. Chang, Solid State Commun. 14, 1163 (1974).
[18]G. S. Painter, D. E. Ellis, and A. R. Lubinsky, Phys. Rev. B 4, 3610 (1971).
[19]M. Cardona, in *Atomic Structure and Properties of Solids*, edited by E. Burstein (Academic, New York, 1972), p. 515.
[20]D. Penn, Phys. Rev. 128, 2093 (1962).
[21]V. Heine and R. O. Jones, J. Phys. C 2, 719 (1969).
[22]D. E. Aspnes and M. Cardona, Phys. Rev. (to be published).
[23]R. A. Roberts and W. C. Walker, Phys. Rev. 161, 730 (1967).
[24]M. Cardona, F. Cerdiera, and T. Fjeldly, Phys. Rev. B 10, 3433 (1974).
[25]B. A. Weinstein and M. Cardona, Phys. Rev. B 8, 2795 (1973).
[26]R. Loudon, Adv. Phys. 13, 434 (1964).
[27]W. Saslow, T. K. Bergstresser, and M. L. Cohen, Phys. Rev. Lett. 16, 354 (1966).
[28]R. M. Martin, Phys. Rev. B 1, 4005 (1970).
[29]M. Chandrasekhar and M. Cardona, Phys. Rev. (to be published).
[30]F. Cerdeira and M. Cardona, Phys. Rev. 5, 1440 (1972).